

# Improved sphaleron decoupling condition and the Higgs coupling constants in the real singlet-extended SM

Kaori Fuyuto\* and Eibun Senaha†

*Department of Physics, Nagoya University, Nagoya 464-8602, Japan*

(Dated: December 3, 2024)

## Abstract

We improve the sphaleron decoupling condition in the real singlet-extended standard model. The sphaleron energy is obtained using the finite temperature one-loop effective potential with daisy resummation. For moderate values of the model parameters, the sphaleron decoupling condition is found to be  $v_C/T_C > (1.1 - 1.2)$ , where  $T_C$  denotes a critical temperature and  $v_C$  is the corresponding vacuum expectation value of the doublet Higgs field at  $T_C$ . We also investigate the deviation of the triple Higgs boson coupling from its standard model value in the region where the improved sphaleron decoupling condition is satisfied. As a result of the improvement, the deviation of the triple Higgs boson coupling gets more enhanced. In a typical case, if the Higgs couplings to the gauge bosons/fermions deviate from the SM values by about 3 (10)%, the deviation of the triple Higgs boson coupling can be as large as about 16 (50)%, which is about 4 (8)% larger than that based on the conventional criterion  $v_C/T_C > 1$ .

---

\* fuyuto@th.phys.nagoya-u.ac.jp

† senaha@eken.phys.nagoya-u.ac.jp

## I. INTRODUCTION

To obtain full knowledge of the Higgs sector is one of the primary goals in collider physics. After the discovery of the Higgs boson at the Large Hadron Collider (LHC) in 2012 [1, 2], much attention is paid to a question whether the Higgs sector is exactly the same as the one predicted by the standard model (SM). Since many new physics models predict an augmented Higgs sector, we may see a new physics signal in precision measurements of the Higgs coupling constants, such as the Higgs couplings to the weak bosons, fermions, and self couplings.

One of the motivations for new physics is a baryon asymmetry of the Universe (BAU). The baryon-to-photon ratio is determined by the cosmic microwave background (CMB) and the big-bang nucleosynthesis (BBN) [3]:

$$\eta_{\text{CMB}} = \frac{n_B}{n_\gamma} = (6.23 \pm 0.17) \times 10^{-10}, \quad (1)$$

$$\eta_{\text{BBN}} = \frac{n_B}{n_\gamma} = (5.1 - 6.5) \times 10^{-10}, \text{ (95\% C.L.)}. \quad (2)$$

To explain the observed value, the so-called Sakharov criteria [4] is needed, i.e., (i) baryon number ( $B$ ) violation, (ii) both  $C$  and  $CP$  violation, (iii) out of thermal equilibrium. It is well known that the last condition in Sakharov criteria, which can be realized if the electroweak phase transition (EWPT) is first order, is not satisfied for the observed Higgs boson mass, 126 GeV. The lattice calculations show that the EWPT in the SM is a smooth crossover [5]. In addition to the above problem,  $CP$  violation that comes from the Cabibbo-Kobayashi-Maskawa matrix [6, 7] is not large enough to generate the sufficient BAU [8].

Although many working mechanisms for generating the BAU exist in the literature, electroweak baryogenesis (EWBG) [9] is one of the most testable scenarios since the relevant energy scale is within our reach, i.e.,  $\mathcal{O}(100)$  GeV. It is expected that ongoing and upcoming experiments on Higgs sector and  $CP$  violation such as electric dipole moments (EDMs) of neutron, atom and molecule can entirely verify or falsify the EWBG hypothesis. Indeed, the EWBG in minimal supersymmetric standard model (MSSM) has been made much unlikely by the LHC data, especially, the results of Higgs signal strengths [10]. On the other hand, the EWBG in other models are not so severely constrained by the current LHC data. In any case, to get the definitive conclusion, theoretical uncertainties have to be minimized. In particular, the improvement of the sphaleron decoupling condition is indispensable. Con-

ventionally, the following rough criterion is frequently used

$$\frac{v_C}{T_C} \gtrsim 1, \quad (3)$$

where  $T_C$  is a critical temperature and  $v_C$  is the corresponding Higgs vacuum expectation value (VEV) at  $T_C$ . Note that the right-hand side also inherently depends on the temperature. To evaluate the right-hand side more precisely, the sphaleron profile and the nucleation temperature ( $T_N$ ) have to be determined. In Ref. [11], the sphaleron energy and zero-mode factors of the fluctuations around the sphaleron are evaluated at  $T_N$  using the finite temperature one-loop effective potential in the MSSM. It is found that the sphaleron decoupling condition is  $v_N/T_N \gtrsim 1.4$ . Therefore, the possible region for the EWBG based on the conventional criterion is optimistically evaluated by about 40%. As demonstrated in [11], viability of the EWBG in the MSSM was already in jeopardy by the refined sphaleron decoupling condition independent of the recent LHC data.

In this paper, we improve the sphaleron decoupling condition and revisit the region where the EWPT is strongly first order in the real singlet-extended SM (rSM). Earlier related work on this subject can be found in Refs. [12–17]. To evaluate the sphaleron decoupling condition, we calculate the sphaleron energy using the finite temperature one-loop effective potential with daisy resummation. We first examine the dependences of the second Higgs mass and the mixing angle between the two Higgs bosons on the sphaleron energy without including the temperature effects, and then scrutinize the temperature effects. With the same effective potential, we compute  $v_C/T_C$  and search for a parameter space that satisfy the improved sphaleron decoupling condition.

We also study relationships between the strength of the strong first-order EWPT and the deviations of the Higgs coupling constants from the SM values. It is known that in the region where the strong first-order EWPT is driven, the significant deviation of the triple Higgs boson coupling from the SM prediction can arise in the two Higgs doublet model [18]. In Ref. [18], it is shown that the deviation can be greater than (10 – 20)% level depending on the magnitude of the  $Z_2$  breaking mass parameter. The degree to which the deviation can occur actually depends on the sphaleron decoupling condition. For instance, if the sphaleron decoupling condition gets more severe, the corresponding deviation of the triple Higgs boson coupling can be more enhanced. In the analysis of [18], the conventional criterion  $v_C/T_C > 1$  was used. In this article, however, we study the deviation of the triple Higgs boson coupling

based on the improved sphaleron decoupling condition.

The paper is organized as follows. In Sec. II, we introduce the model and discuss the vacuum structure of this model. In Sec. III, we present standard formulas for studying the EWPT and classify the patterns of the EWPT. The sphaleron decoupling condition is given in Sec. IV. Subsequently, a typical example is given in order to see the magnitude of the sphaleron energy in this model. Our main results are presented in Sec. V, and Sec. VI is devoted to conclusions and discussion.

## II. THE MODEL

We consider a minimal extension of the SM that includes a gauge singlet real scalar  $S$ . The most general renormalizable scalar potential is given by

$$\begin{aligned} V_0 = & -\mu_H^2 H^\dagger H + \lambda_H (H^\dagger H)^2 \\ & + \mu_{HS} H^\dagger H S + \frac{\lambda_{HS}}{2} H^\dagger H S^2 \\ & + \mu_S^3 S + \frac{m_S^2}{2} S^2 + \frac{\mu'_S}{3} S^3 + \frac{\lambda_S}{4} S^4, \end{aligned} \quad (4)$$

where  $H$  is the SU(2) doublet Higgs field. After two scalar fields  $H$  and  $S$  get the VEVs ( $v$  and  $v_S$ ), they are cast into the form

$$H(x) = \begin{pmatrix} G^+(x) \\ \frac{1}{\sqrt{2}}(v + h(x) + iG^0(x)) \end{pmatrix}, \quad S(x) = v_S + s(x). \quad (5)$$

The minimization (tadpole) conditions of the scalar potential can be written as

$$\begin{aligned} \mu_H^2 &= \lambda_H v^2 + \mu_{HS} v_S + \frac{\lambda_{HS}}{2} v_S^2, \\ m_S^2 &= -\frac{\mu_S^3}{v_S} - \mu'_S v_S - \lambda_S v_S^2 - \frac{\mu_{HS}}{2} \frac{v^2}{v_S} - \frac{\lambda_{HS}}{2} v^2. \end{aligned} \quad (6)$$

The mass matrix of  $h$  and  $s$  (denoted as  $\mathcal{M}_H^2$ ) has the 2-by-2 form. The mass eigenvalues ( $m_{H_1, H_2}^2$ ) are obtained by diagonalizing  $\mathcal{M}_H^2$  with an orthogonal matrix  $O(\alpha)$

$$\mathcal{M}_H^2 = \begin{pmatrix} (\mathcal{M}_H)_{11}^2 & (\mathcal{M}_H)_{12}^2 \\ (\mathcal{M}_H)_{21}^2 & (\mathcal{M}_H)_{22}^2 \end{pmatrix} = \begin{pmatrix} \cos \alpha & -\sin \alpha \\ \sin \alpha & \cos \alpha \end{pmatrix} \begin{pmatrix} m_{H_1}^2 & 0 \\ 0 & m_{H_2}^2 \end{pmatrix} \begin{pmatrix} \cos \alpha & \sin \alpha \\ -\sin \alpha & \cos \alpha \end{pmatrix}, \quad (7)$$

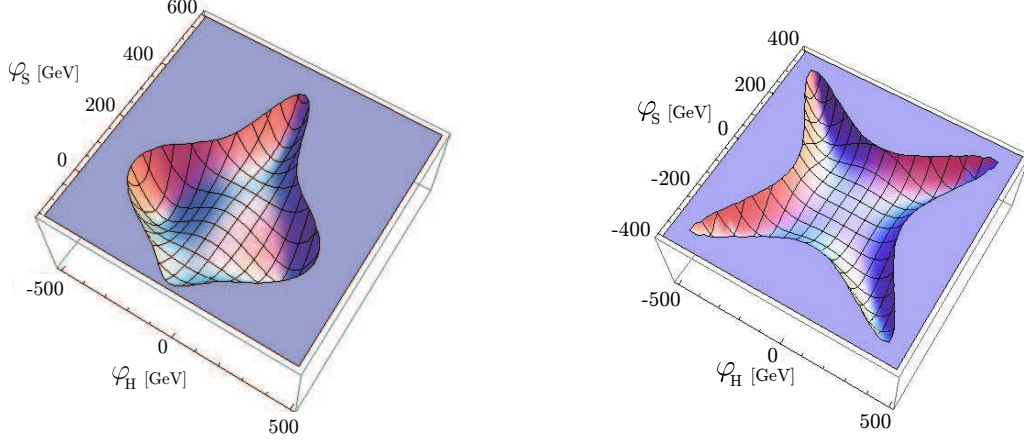


FIG. 1. The shape of the tree-level potential,  $V_0(\varphi_H, \varphi_S)$  and  $V_0^{Z_2}(\varphi_H, \varphi_S)$  as functions of  $\varphi_H$  and  $\varphi_S$  in left and right figures, respectively. In the left (right) figure, we take  $m_{H_1} = 125.5$  GeV,  $m_{H_2} = 150$  (500) GeV,  $v_S = 100$  (200) GeV,  $\alpha = 0^\circ$  ( $38^\circ$ ),  $\mu'_S = -30$  (0) GeV, and  $\mu_{HS} = -80$  (0) GeV.

where the value of  $\alpha$  is defined in the range  $-\pi/4 \leq \alpha \leq \pi/4$ , and each mass matrix element is respectively given by

$$\begin{aligned} (\mathcal{M}_H)_{11}^2 &= 2\lambda_H v^2, \\ (\mathcal{M}_H)_{12}^2 &= \mu_{HS}v + \lambda_{HS}v + \lambda_{HS}vv_S, \\ (\mathcal{M}_H)_{22}^2 &= -\frac{\mu_S^3}{v_S} + \mu'_S v_S + 2\lambda_S v_S^2 - \frac{\mu_{HS}}{2} \frac{v^2}{v_S}, \end{aligned} \quad (8)$$

where we used the tadpole conditions (6).

The tree-level effective potential takes the form

$$\begin{aligned} V_0(\varphi_H, \varphi_S) &= \frac{\lambda_H}{4}(\varphi_H^4 - 2v_H^2\varphi_H^2) + \frac{\mu_{HS}}{2} \left( \varphi_H^2\varphi_S - \varphi_H^2v_S - \frac{v_H^2\varphi_S^2}{2v_S} \right) \\ &+ \frac{\lambda_{HS}}{4}(\varphi_H^2\varphi_S^2 - \varphi_H^2v_S^2 - v_H^2\varphi_S^2) + \mu_S^3 \left( \varphi_S - \frac{\varphi_S^2}{2v_S} \right) \\ &+ \frac{\mu'_S}{3} \left( \varphi_S^3 - \frac{3}{2}v_S\varphi_S^2 \right) + \frac{\lambda_S}{4}(\varphi_S^4 - 2v_S^2\varphi_S^2), \end{aligned} \quad (9)$$

where  $\varphi$  and  $\varphi_S$  are the constant background fields of the doublet and singlet Higgses. The Higgs potential has to satisfy the unbounded from below condition

$$\lambda_H > 0, \quad \lambda_S > 0, \quad 4\lambda_H\lambda_S > \lambda_{HS}^2, \quad (10)$$

where the last condition is needed if  $\lambda_{HS} < 0$ . If we impose a  $Z_2$  symmetry, the Higgs

potential (4) is reduced to

$$V_0^{Z_2} = -\mu_H^2 H^\dagger H + \lambda_H (H^\dagger H)^2 + \frac{\lambda_{HS}}{2} H^\dagger H S^2 + \frac{m_S^2}{2} S^2 + \frac{\lambda_S}{4} S^4. \quad (11)$$

In Fig. 1, we show the representative examples of  $V_0(\varphi_H, \varphi_S)$  and  $V_0^{Z_2}(\varphi_H, \varphi_S)$ . In the left (right) figure, we set  $m_{H_1} = 125.5$  GeV,  $m_{H_2} = 150$  (500) GeV,  $v_S = 100$  (200) GeV,  $\alpha = 0^\circ$  ( $38^\circ$ ),  $\mu'_S = -30$  (0) GeV, and  $\mu_{HS} = -80$  (0) GeV. The both Higgs potentials are symmetric about  $\varphi_H$  axis. On top of this,  $V_0^{Z_2}(\varphi_H, \varphi_S)$  is also symmetric about  $\varphi_S$  axis because of the  $Z_2$  symmetry. As discussed in Ref. [19], the vacuum structures at the zero temperature may provide some information about the patterns of the phase transitions. In the left Higgs potential, there is a local minimum in the  $\varphi_S$  axis. As we discuss later, the phase transition can occur twice, i.e., the transition from the origin to the local minimum along the  $\varphi_S$  axis, followed by the transition from there to our vacuum as the temperature decreases. In the right case, on the other hand, the phase transition may proceed once, i.e., the transition from the origin to our vacuum directly. We argue various patterns of the phase transitions in the next section.

At the tree level, the interactions of  $H_1$  and  $H_2$  with  $Z$  and  $W$  bosons are

$$\mathcal{L}_{\text{HVV}} = \frac{1}{v} (\cos \alpha H_1 - \sin \alpha H_2) (2m_W^2 W_\mu^+ W^{-\mu} + m_Z^2 Z_\mu Z^\mu), \quad (12)$$

and the interactions with quarks  $f$  are

$$\mathcal{L}_{\text{Yukawa}} = - \sum_f \frac{m_f}{v} (\cos \alpha H_1 - \sin \alpha H_2) \bar{f} f. \quad (13)$$

We define the Higgs couplings to gauge bosons and fermions normalized to the corresponding SM ones as

$$\kappa_V = \frac{g_{H_1 VV}}{g_{hVV}^{\text{SM}}} = \cos \alpha, \quad \kappa_F = \frac{g_{H_1 ff}}{g_{hff}^{\text{SM}}} = \cos \alpha. \quad (14)$$

Since  $\kappa_V$  and  $\kappa_F$  are the same value in the rSM, we collectively denote them as  $\kappa$  in the following.

### III. ELECTROWEAK PHASE TRANSITION

In addition to the tree-level potential (4), we include the one-loop Coleman-Weinberg potential at zero temperature [20, 21], which is given by

$$V_1(\varphi_H, \varphi_S) = \sum_i n_i \frac{\bar{m}_i^4(\varphi_H, \varphi_S)}{64\pi^2} \left( \ln \frac{\bar{m}_i^2(\varphi_H, \varphi_S)}{\mu^2} - c_i \right), \quad (15)$$

where  $\mu$  is a renormalization scale, which will be set at  $v$ .  $\bar{m}_i$  is the background field dependent mass, and the numerical constant  $c_i$  is  $3/2$  ( $5/6$ ) for scalar and fermion (gauge boson).  $n_i$  are the degrees of freedom of particle species  $i$  ( $= H_{1,2}, G^0, G^\pm, W, Z, t, b$ ), which is, respectively, given by

$$n_{H_1} = n_{H_2} = n_{G^0} = 1, \quad n_{G^\pm} = 2, \quad n_W = 2 \cdot 3, \quad n_Z = 3, \quad n_t = n_b = -4N_c, \quad (16)$$

where  $N_c$  is the number of color.

The finite temperature component of the one-loop effective potential can be written as

$$V_1(\varphi_H, \varphi_S, T) = \sum_i n_i \frac{T^4}{2\pi^2} I_{B,F} \left( \frac{\bar{m}_i^2(\varphi_H, \varphi_S)}{T^2} \right), \quad (17)$$

where

$$I_{B,F}(a^2) = \int_0^\infty dx \, x^2 \ln \left( 1 \mp e^{-\sqrt{x^2 + a^2}} \right), \quad (18)$$

with the upper (lower) sign for bosons (fermions). If  $T$  is high compared to  $m_i(\varphi_H, \varphi_S)$ ,  $I_{B,F}$  can be expressed as [22]

$$\begin{aligned} I_B(a^2) &= -\frac{\pi^4}{45} + \frac{\pi^2}{12}a^2 - \frac{\pi}{6}(a^2)^{3/2} - \frac{a^4}{32} \ln \left( \frac{a^2}{\alpha_B} \right) + \dots, \\ I_F(a^2) &= \frac{7\pi^2}{360} - \frac{\pi^2}{24}a^2 - \frac{a^4}{32} \ln \left( \frac{a^2}{\alpha_F} \right) + \dots. \end{aligned} \quad (19)$$

where  $\log \alpha_B = 2 \log 4\pi + 3/2 - 2\gamma_E$ ,  $\log \alpha_F = 2 \log \pi + 3/2 - 2\gamma_E$ . Moreover, in order to improve the calculation of the effective potential, we include the so-called daisy contributions [23]

$$V_{\text{daisy}}(\varphi_H, \varphi_S, T) = - \sum_j n_j \frac{T}{12\pi} \left[ \{ \bar{M}_j^2(\varphi_H, \varphi_S, T) \}^{3/2} - \{ \bar{m}_j^2(\varphi_H, \varphi_S) \}^{3/2} \right], \quad (20)$$

where  $\bar{M}_j^2$  are the thermally corrected boson masses

$$\bar{M}_j^2(\varphi_H, \varphi_S, T) = \bar{m}_j^2(\varphi_H, \varphi_S) + \Pi_j(T), \quad (21)$$

and  $\Pi_j(T)$  is the finite temperature mass functions given in Refs. [16, 23]. Although the mass-squared values of the scalar and Nambu-Goldstone bosons can be negative, the above daisy contributions can compensate for them at high temperature. The full effective potential at finite temperature is given by

$$V_{\text{eff}}(\varphi_H, \varphi_S, T) = V_0(\varphi_H, \varphi_S) + V_1(\varphi_H, \varphi_S) + V_1(\varphi_H, \varphi_S, T) + V_{\text{daisy}}(\varphi_H, \varphi_S, T). \quad (22)$$

Phases	Order Parameters
EW	$v = 246 \text{ GeV}, v_S \neq 0$
SYM	$v = 0, v_S = 0$
I, I'	$v = 0, v_S \neq 0$
II	$v \neq 0, v_S = 0$

TABLE I. Various phases in the rSM.

For the first-order EWPT, the effective potential (22) needs to have two degenerate minima at the critical temperature  $T_C$ . The VEVs at  $T_C$  are denoted as

$$v_C = \lim_{T \uparrow T_C} v(T_C), \quad v_{SC} = \lim_{T \uparrow T_C} v_S(T_C), \quad v_{SC}^{\text{sym}} = \lim_{T \downarrow T_C} v_S(T_C), \quad (23)$$

where the up (down) arrows indicate that  $T$  approaches  $T_C$  from below (above). Since the numerical evaluations of  $I_B$  and  $I_F$  are time consuming, we replace them with the fitting functions adopted in Ref. [11]. The errors of the fitting functions are less than  $10^{-6}$  for any  $a^2$ , which is sufficient for our numerical evaluations.

Here, we explain how the EWPT proceeds in the rSM. At high temperatures,  $\text{SU}(2) \times \text{U}(1)_Y$  gauge symmetry is restored. However, as the temperature goes down, the symmetric phase (SYM) is no longer the vacuum, and eventually the electroweak phase (EW) becomes the global minimum. In general, this transition occurs by multi-steps. The various phases that occurs at the intermediate stage are listed in Table I. As discussed in [19], there are four types of the transitions. We show each path of the transitions in Fig. 2. In type C,  $v$  firstly has a nonzero value, and then  $v_S$  starts to grow up. In type A, the transition occurs from SYM to I phase, followed by the transition  $\text{I} \rightarrow \text{EW}$  with an almost constant  $v_S$ , In type B, the transition is the same as type A but with varying  $v_S$  in the second transition. In type D, SYM goes to EW phase directly. In principle, we can consider a case in which II phase corresponds to our vacuum. However, we do not pursue this case here for simplicity.

#### IV. SPHALERON DECOUPLING CONDITION

In the EWBG mechanism, the BAU is generated through the sphaleron process in the symmetric phase during the EWPT. In order to leave the BAU, the sphaleron process has



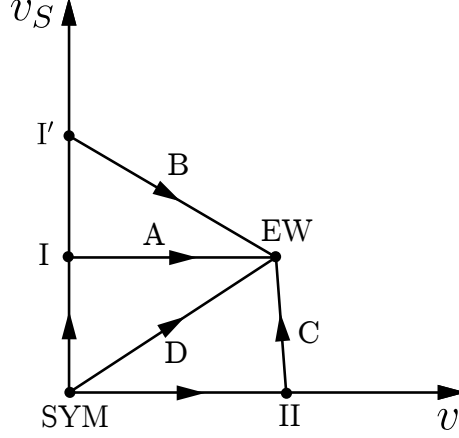


FIG. 2. The diverse patterns of the EWPT.

to be decoupled right after the EWPT. Namely, the  $B$ -changing rate in the broken phase ( $\Gamma_B^{(b)}$ ) must be less than the Hubble constant ( $H(T)$ )

$$\Gamma_B^{(b)}(T) \simeq (\text{prefactor}) e^{-E_{\text{sph}}(T)/T} < H(T) \simeq 1.66 \sqrt{g_*(T)} T^2 / m_{\text{P}} \quad (24)$$

where  $E_{\text{sph}}(T)$  is the sphaleron energy,  $g_*$  counts degrees of freedom of relativistic particles in the thermal plasma ( $g_* = 107.75$  in the rSM) and  $m_{\text{P}}$  denotes the Planck mass ( $1.22 \times 10^{19}$  GeV). The prefactor denotes a fluctuation determinant around the sphaleron (see, e.g., [11, 24]). From Eq. (24), it follows that

$$\frac{v(T)}{T} > \frac{g_2}{4\pi\mathcal{E}(T)} \left[ 42.97 + \ln \mathcal{N} - 2 \ln \left( \frac{T}{100 \text{ GeV}} \right) + \dots \right] \equiv \zeta_{\text{sph}}(T), \quad (25)$$

where we use  $E_{\text{sph}}(T) = 4\pi v(T)\mathcal{E}(T)/g_2$  with  $g_2$  being the SU(2) gauge coupling constant.  $\mathcal{N}$  denotes the translational and rotational zero mode factors of the fluctuations about the sphaleron. Note that the dominant contribution in  $\zeta_{\text{sph}}(T)$  comes from  $\mathcal{E}(T)$  while the next-to-leading term may be  $\ln \mathcal{N}$ . In the MSSM,  $\ln \mathcal{N}$  typically amounts to 10% [11]. The last term can become relevant if  $T_C$  is significantly lower than 100 GeV. As is well known, this can happen in the rSM. In the current investigation, we exclusively focus on the calculation of  $\mathcal{E}(T)$  by using Eq.(22) and evaluate Eq.(25) without the  $\ln \mathcal{N}$  term as a first step toward to the complete analysis. It should be noticed that the EWPT starts to develop after the nucleation of Higgs bubbles. It is thus better to evaluate Eq.(25) at such a nucleation temperature ( $T_N$ ) rather than at  $T_C$ . In this paper, however, we adopt  $v(T_C)/T_C > \zeta_{\text{sph}}(T_C)$  as the sphaleron decoupling criterion for simplicity.

We closely follow the method given in Refs. [25–27] to obtain the sphaleron solution (for earlier studies on the sphaleron solutions in the rSM, see, i.e., [28]). Since  $U(1)_Y$  contributions are sufficiently small [29], we employ the spherically symmetric ansatz. Specifically, we consider the configuration space spanned by the followings

$$A_i(\mu, r, \theta, \phi) = -\frac{i}{g_2} f(r) \partial_i U(\mu, \theta, \phi) U^{-1}(\mu, \theta, \phi), \quad (26)$$

$$H(\mu, r, \theta, \phi) = \frac{v}{\sqrt{2}} \left[ (1 - h(r)) \begin{pmatrix} 0 \\ e^{-i\mu} \cos \mu \end{pmatrix} + h(r) U(\mu, \theta, \phi) \begin{pmatrix} 0 \\ 1 \end{pmatrix} \right], \quad (27)$$

$$S(\mu, r, \theta, \phi) = v_S k(r), \quad (28)$$

where  $A_i$  is SU(2) gauge fields, and  $U$  is defined as

$$U(\mu, \theta, \phi) = \begin{pmatrix} e^{i\mu}(\cos \mu - i \sin \mu \cos \theta) & e^{i\phi} \sin \mu \sin \theta \\ -e^{-i\phi} \sin \mu \sin \theta & e^{-i\mu}(\cos \mu + i \sin \mu \cos \theta) \end{pmatrix}, \quad (29)$$

with  $\mu \in [0, \pi]$ .  $U(\mu, \theta, \phi)$  is noncontractible since  $\pi_3(\text{SU}(2)) \simeq \mathbb{Z}$ .  $\mu$  parameterizes the least energy path connecting between the topologically different vacua. The configuration at  $\mu = \pi/2$  corresponds to the sphaleron.

The energy functional in  $A_0 = 0$  is given by

$$E[H, S] = \int d^3 \mathbf{x} \left[ \frac{1}{4} F_{ij}^a F_{ij}^a + (D_i H)^\dagger D_i H + \frac{1}{2} \partial_i S \partial_i S + V_{\text{eff}}(H, S, T) \right], \quad (30)$$

where the tree-level potential is replaced with the one-loop corrected one in order to incorporate the high-order effects. For  $\mu = \pi/2$ , one gets

$$E_{\text{sph}}[f, h, k] = \frac{4\pi v}{g_2} \int_0^\infty d\xi \left[ 4 \left( \frac{df}{d\xi} \right)^2 + \frac{8}{\xi^2} (f - f^2)^2 + \frac{\xi^2}{2} \left( \frac{dh}{d\xi} \right)^2 + h^2 (1 - f)^2 + \frac{\xi^2}{2} \frac{v_S^2}{v^2} \left( \frac{dk}{d\xi} \right)^2 + \frac{\xi^2}{g_2^2 v^4} V_{\text{eff}}(h, k, T) \right], \quad (31)$$

where  $\xi = g_2 v r$ . From Eq. (31), the equations of motion are found to be

$$\frac{d^2 f}{d\xi^2} = \frac{2}{\xi^2} f(1 - f)(1 - 2f) - \frac{1}{4} h^2 (1 - f), \quad (32)$$

$$\frac{d}{d\xi} \left( \xi^2 \frac{dh}{d\xi} \right) = 2h(1 - f)^2 + \frac{\xi^2}{g_2^2 v^4} \frac{\partial V_{\text{eff}}}{\partial h}, \quad (33)$$

$$\frac{d}{d\xi} \left( \xi^2 \frac{dk}{d\xi} \right) = \frac{\xi^2}{g_2^2 v^2 v_S^2} \frac{\partial V_{\text{eff}}}{\partial k}. \quad (34)$$

We solve the above equations with the following boundary conditions

$$\lim_{\xi \rightarrow 0} f(\xi) = 0, \quad \lim_{\xi \rightarrow 0} h(\xi) = 0, \quad \lim_{\xi \rightarrow 0} k'(\xi) = 0, \quad (35)$$

$$\lim_{\xi \rightarrow \infty} f(\xi) = 1, \quad \lim_{\xi \rightarrow \infty} h(\xi) = 1, \quad \lim_{\xi \rightarrow 0} k(\xi) = 1. \quad (36)$$

Before going to the detailed analysis of the EWPT and the sphaleron decoupling condition, we demonstrate how  $\mathcal{E}$  depends on model parameters. At this point, we use the zero-temperature one-loop effective potential to extract the non-temperature dependence, and the full analysis is performed in Sec. V.

In the left panel of Fig. 3,  $\mathcal{E}$  is shown as a function of  $\alpha$ . We take  $m_{H_1} = 125.5$  GeV,  $m_{H_2} = 500$  GeV,  $v_S = 200$  GeV and  $\mu_S = \mu'_S = \mu_{HS} = 0$  GeV as an example. We can see that  $\mathcal{E}$  gets larger as  $\alpha$  increases. It rises about 5% from  $\alpha = 0^\circ$  to  $\alpha \simeq 45^\circ$ . To understand this behavior, we also show  $\lambda_H$ ,  $\lambda_S$  and  $\lambda_{HS}$  in the right panel of Fig. 3. Those coupling are determined after fixing  $m_{H_{1,2}}$  and  $\alpha$ .  $\lambda_H$  has to increase according to the rise of  $\alpha$  to keep the value of  $m_{H_1}$  fixed. On the other hand,  $\lambda_S$  behaves oppositely as it should be. We can see that the increment of  $\mathcal{E}$  is due to the enhancement of  $\lambda_H$ . This correlation is already shown within the SM [26], and the same behavior is observed in the rSM. We also find the mild dependence of  $m_{H_2}$  on  $\mathcal{E}(0)$ , which is again essentially because of the increase or decrease of  $\lambda_H$ .

## V. NUMERICAL ANALYSIS

In this section, we perform the numerical analysis. In the rSM, there are 8 parameters in the tree-level potential:

$$\mu_H^2, m_S^2, \mu_S, \mu'_S, \mu_{HS}, \lambda_H, \lambda_{HS}, \lambda_S. \quad (37)$$

In our analysis,  $\mu_H^2$ ,  $m_S^2$ ,  $\lambda_H$ ,  $\lambda_S$  and  $\lambda_{HS}$  are traded with  $v$ ,  $v_S$ ,  $m_{H_1}$ ,  $m_{H_2}$  and  $\alpha$ . This replacement can be done by solving the following coupled equations:

$$\frac{1}{v} \left\langle \frac{\partial V_{\text{eff}}}{\partial \varphi_H} \right\rangle = \frac{1}{v_S} \left\langle \frac{\partial V_{\text{eff}}}{\partial \varphi_S} \right\rangle = 0, \quad (38)$$

$$(\mathcal{M}_H^2)_{11} - m_{H_1}^2 \cos^2 \alpha - m_{H_2}^2 \sin^2 \alpha = 0, \quad (39)$$

$$(\mathcal{M}_H^2)_{22} - m_{H_1}^2 \sin^2 \alpha - m_{H_2}^2 \cos^2 \alpha = 0, \quad (40)$$

$$(\mathcal{M}_H^2)_{12} - (m_{H_1}^2 - m_{H_2}^2) \sin \alpha \cos \alpha = 0. \quad (41)$$

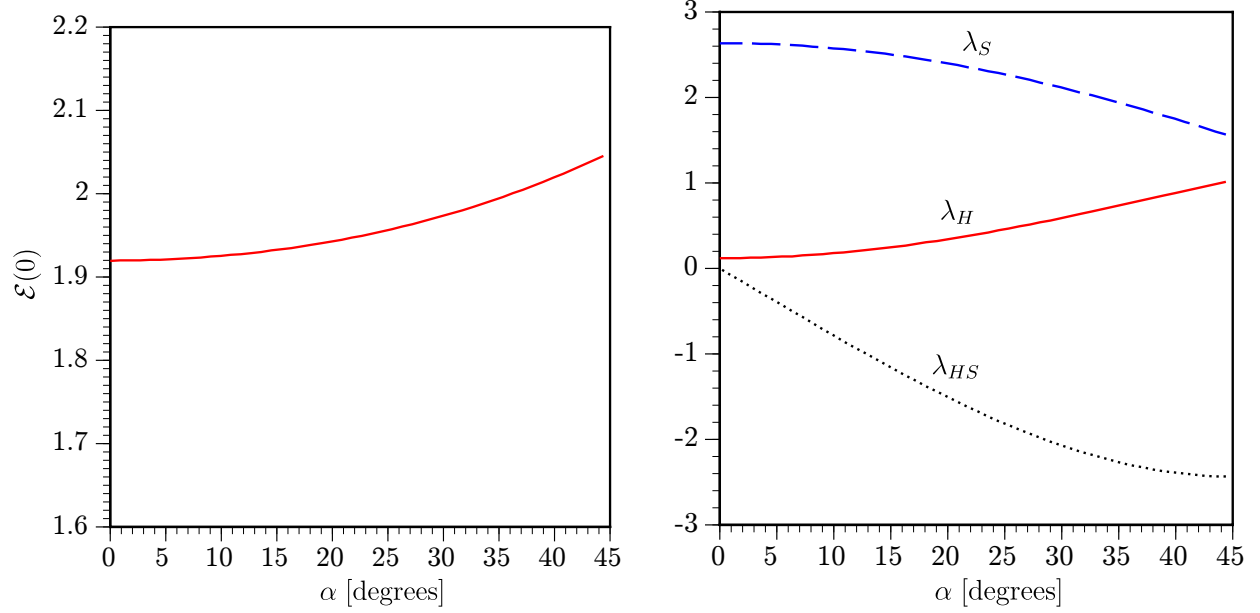


FIG. 3. The sphaleron energy (left panel) and  $\lambda_{H,S,HS}$  (right panel) are plotted as a function of  $\alpha$ . We set  $m_{H_1} = 125.5$  GeV,  $m_{H_2} = 500$  GeV,  $v_S = 200$  GeV and  $\mu_S = \mu'_S = \mu_{HS} = 0$  GeV.

where we take  $m_{H_1} = 125.5$  GeV and  $v = 1/(2^{1/4}\sqrt{G_F})(\simeq 246$  GeV) with  $G_F$  being the Fermi coupling constant.  $\langle X \rangle$  denotes that  $X$  is evaluated in the vacuum,  $\varphi_H = v$  and  $\varphi_S = v_S$ . Since the Nambu-Goldstone boson loop contributions that have to be treated with some care are numerically unimportant, and thus we will not take them into account in the current investigation. Throughout our analysis, we take  $\mu_S = 0$ .

As mentioned in Introduction, the EWPT in the SM is not strongly first order for the observed Higgs mass. In order to circumvent this, the Higgs potential has to be altered by the doublet-singlet Higgs mixing terms (H-S mixing parameters :  $\mu_{HS}$  and  $\lambda_{HS}$ ). Here, we consider the following 2 cases:

- (i) one H-S mixing parameters case  $[(\lambda_{HS} \neq 0, \mu_{HS} = 0) \text{ or } (\lambda_{HS} = 0, \mu_{HS} \neq 0)]$ ,
- (ii) two H-S mixing parameters case  $[\lambda_{HS} \neq 0, \mu_{HS} \neq 0]$ .

Without going to the detailed investigation, we can foresee the latter case has larger window to the strong first-order EWPT. We conduct the analysis based on the improved sphaleron decoupling condition.

### A. One H-S mixing parameters case

Here, we consider Case (i) with  $\lambda_{HS} \neq 0$  and  $\mu_{HS} = 0$ .<sup>1</sup> In Figure 4, we show an allowed region where the following condition is achieved in the  $(m_{H_2}, \alpha)$  plane,

$$\frac{v_C}{T_C} > \zeta_{\text{sph}}(T_C). \quad (42)$$

We here take  $m_{H_1} = 125.5$  GeV,  $v_S = 200$  GeV, and  $\mu'_S = \mu_{HS} = 0$  GeV.<sup>2</sup> It is found that only large values of  $\alpha$  and  $m_{H_2}$  are allowed. In addition, the sign of  $\alpha$  is need to be positive, and thus  $\lambda_{HS}$  is negative, for the first-order phase transition as discussed in [13]. However, these large values of  $\alpha$  and  $m_{H_2}$  receive stringent constraints from the EW precision tests [31, 32]. According to Ref. [33],  $\alpha$  is less than about  $23^\circ$  for  $m_{H_2} \gtrsim 400$  GeV. Moreover, the recent LHC data indicates that the value of  $\kappa$  is bounded as follows [34, 35],

$$\kappa_V = 1.15^{+0.08}_{-0.08} \text{ (ATLAS)}, \quad \kappa_V = 0.81 - 0.97 \text{ (CMS)}. \quad (43)$$

Thus, it seems difficult to have the strong first-order phase transition in the spontaneously broken  $Z_2$  model. However, there may be a way out. If we consider the II phase as the EW phase,  $\alpha = 0$  in such a vacuum since  $v_S = 0$ . In this case, the transition  $\text{SYM} \rightarrow \text{I(I')} \rightarrow \text{II}$  can induce the strong first-order phase transition, so the above experimental constraints are no longer stringent. For a recent study on such a possibility, see, for instance, [17].

Although the successful region in the  $Z_2$  model is strongly disfavored by the LHC data and EW precision tests, we give an example that shows how the EWPT is strengthen and which type of the EWPT can be realized. More importantly, the typical size of  $\zeta_{\text{sph}}(T_C)$  in the rSM is epitomized. The example is shown in Fig. 5 in which  $m_{H_2} = 500$  GeV is chosen. In the left panel, the Higgs VEVs at  $T_C$  are displayed. At around  $\alpha = 34^\circ$ ,  $v_{SC}^{\text{sym}}$  becomes zero, so the type of the EWPT is changed into D from B. It is found that the conventional decoupling criterion  $v_C/T_C > 1$  is satisfied for  $\alpha \gtrsim 35^\circ$ . The right panel shows  $v_C/T_C$  and  $\zeta_{\text{sph}}(T_C)$  in the narrowed  $\alpha$  range. The crossing point occurs at around  $\alpha = 37.2^\circ$  which is somewhat stronger than the bound obtained by the conventional criterion. We also find that for  $\alpha \gtrsim 38^\circ$ , the EWPT is changed into type C which is weakly first order as expected. In summary, the EWPT in Case (i) can be strongly first order due to the sizable  $\alpha$ , equivalently sizable  $\lambda_{HS}$  with a negative sign, and its PT property is type D.

<sup>1</sup> A representative example with  $\lambda_{HS} = 0$  and  $\mu_{HS} \neq 0$  is given in Table II.

<sup>2</sup> We allow a small  $Z_2$  breaking term to avoid the domain wall problem [30], so what we call  $Z_2$  model is approximate one.

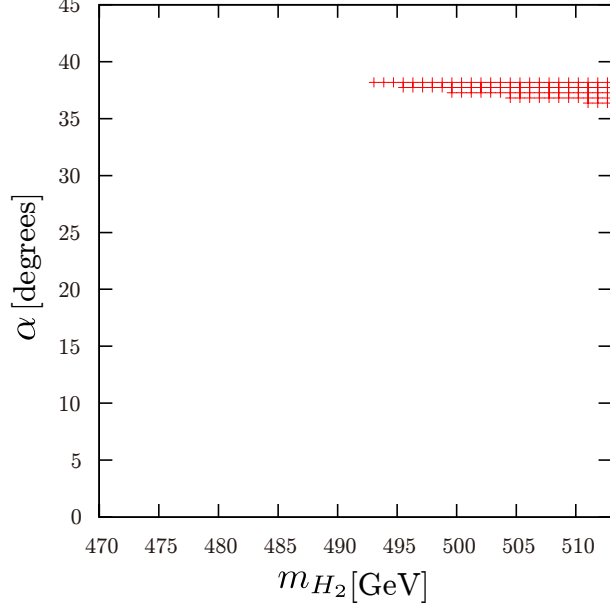


FIG. 4. The possible region for the strong first-order phase transition in Case (i). In this figure, we set  $m_{H_1} = 125.5$  GeV,  $v_S = 200$  GeV, and  $\mu'_S = \mu_{HS} = \mu_S = 0$  GeV.

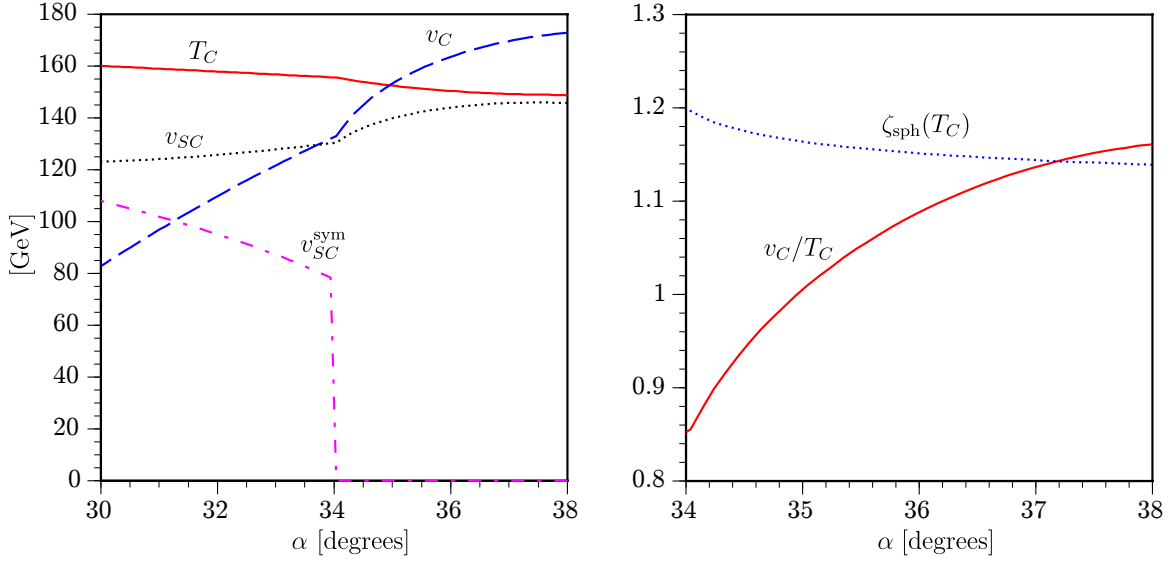


FIG. 5. The Higgs VEVs at  $T_C$  (Left panel) and  $v_C/T_C$  and  $\zeta_{\text{sph}}$  (right panel) are presented as function of  $\alpha$  in Case (i).

## B. Two H-S mixing parameters case

We move on to analyze Case (ii). Figure 6 shows the possible allowed region for the strong first-order phase transition in Case (ii). In this figure, we set  $m_{H_1} = 125.5$  GeV,

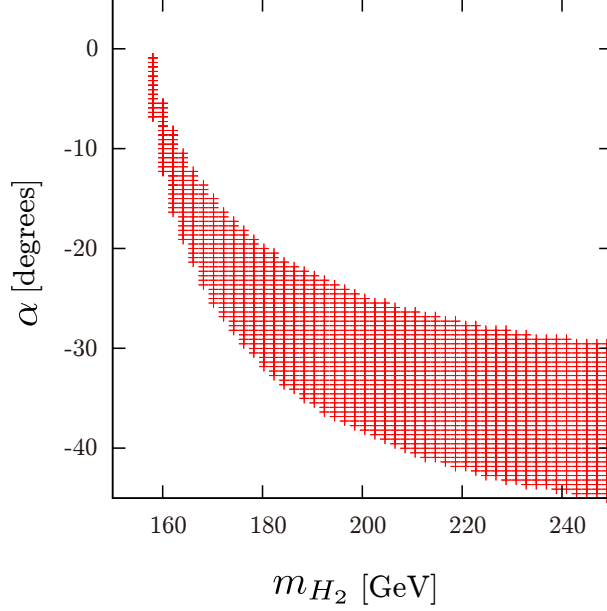


FIG. 6. The possible region for the strong first-order phase transition in Case (ii). In this figure, we set  $m_{H_1} = 125.5$  GeV,  $v_S = 90$  GeV,  $\mu'_S = -30$  GeV,  $\mu_{HS} = -80$  GeV and  $\mu_S = 0$  GeV.

$v_S = 90$  GeV,  $\mu'_S = -30$  GeV,  $\mu_{HS} = -80$  GeV. As you can see, Figure 6 has the larger possible regions compared to the one in  $Z_2$  model. It is found that there is the upper limit of  $m_{H_2}$ , if we fix  $\alpha$ . For example, at  $\alpha = -15.6^\circ$ , the successful range of  $m_{H_2}$  is less than about 170 GeV. Further,  $\alpha$  is restricted to the negative region in order to realize the strong first-order phase transition in the chosen parameter set.

We look into more detail of the EWPT properties in Case (ii). In the left panel of Fig. 7, the VEVs at  $T_C$  are plotted in the range  $-25^\circ \leq \alpha \leq -7^\circ$ , setting  $m_{H_2} = 170$  GeV. We can see that  $v_C/T_C$  becomes enhanced as  $\alpha$  decreases. In this region,  $|v_{SC}^{\text{sym}} - v_{SC}|$  is significantly large, so the PT property is type B. Conversely,  $|v_{SC}^{\text{sym}} - v_{SC}|$  gets smaller for a smaller  $\alpha$ , and the PT is eventually reduced to type A which is weakly first order as explicitly shown here. In the right panel of Fig. 7, we plot  $\lambda_H$ ,  $\lambda_S$  and  $\lambda_{HS}$  in the same  $\alpha$  range. A relatively large  $\lambda_{HS}$  is needed to drive the EWPT to be strongly first order. Unlike the  $Z_2$  model, the sign of  $\lambda_{HS}$  is not necessarily negative in this case. However, we should note that  $\mu_{HS}$  has to be negative.

Now we discuss  $\zeta_{\text{sph}}$  in the above benchmark point. We first scrutinize the sphaleron energy with and without a temperature effect. In the left panel of Fig. 8, we give  $\mathcal{E}(0)$  and  $\mathcal{E}(T_C)$ . The slight rise of  $\mathcal{E}(0)$  with a decreasing  $\alpha$  is mainly due to the corresponding

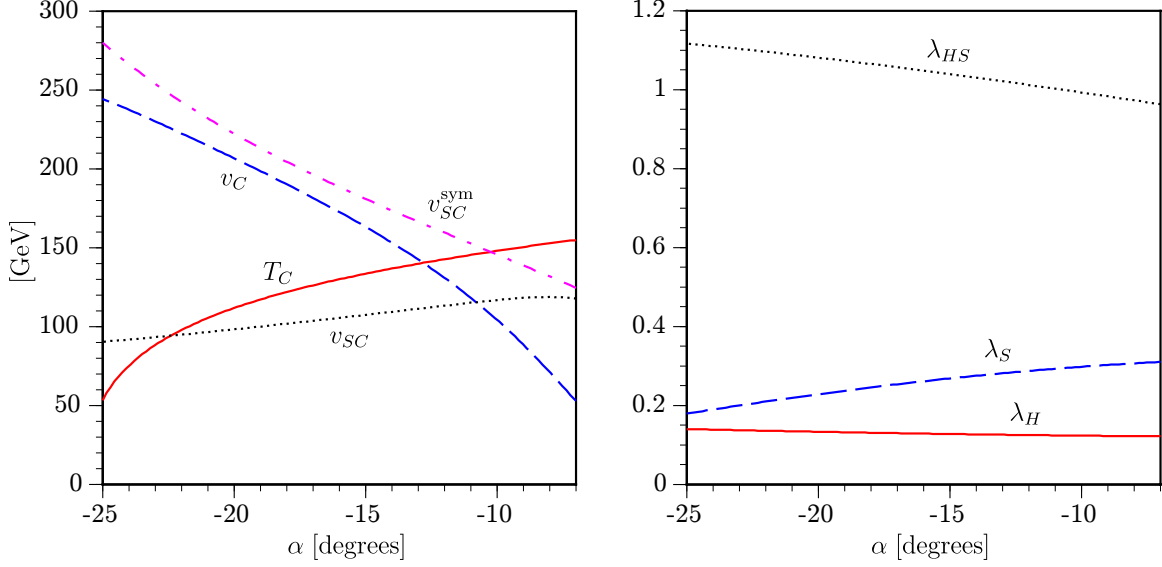


FIG. 7. The Higgs VEVs at  $T_C$  (left panel) and  $\lambda_{H,S,HS}$  (right panel) are shown as a function of  $\alpha$  in Case (ii).

value of  $\lambda_H$  which has the same rising behavior as shown in the right panel of Fig. 7. On the other hand,  $\mathcal{E}(T_C)$  has a significant temperature dependence. It is found that  $\mathcal{E}(T_C) < \mathcal{E}(0)$ . The simple argument is as follows. In general, at finite temperatures the energy difference between the broken phase and the symmetric phase ( $v = 0$  GeV) is smaller than that at the zero temperature, namely,  $V_{\text{eff}}$  appearing in Eq. (31) gets smaller as the temperature increases. Correspondingly, the gradient energy becomes smaller to balance with the potential energy for the classical solution to exist. The right panel of Fig. 8 quantitatively supports the above argument. Here, we plot  $f(\xi)$ ,  $h(\xi)$  and  $k(\xi)$  at  $T = 0$  GeV and  $T_C$ , choosing  $\alpha = -10^\circ$ . The straight (dotted) lines denote  $f(\xi)$ ,  $h(\xi)$  and  $k(\xi)$  at  $T = T_C(0)$ . As can be seen, the gradients of the doublet Higgs and the gauge field are lowered at  $T_C$ . On the other hand, the singlet Higgs does not yield a significant contribution to the gradient energy in Eq. (31).

Now let us estimate  $\zeta_{\text{sph}}(T)$  with the sphaleron energies obtained above. The left panel of Fig. 9 shows  $\zeta_{\text{sph}}(T_C)$  and  $\zeta_{\text{sph}}(0)$  as a function of  $\alpha$ . As discussed in Sec. IV, the smaller  $\mathcal{E}$  gives the larger  $\zeta_{\text{sph}}$ . The slight rise at around  $\alpha = -25^\circ$  is due to the third term on the right-hand side of Eq. (25). In this region,  $T_C$  rapidly gets lowered and can be as small as around 50 GeV as shown in the left panel of Fig. 7, giving rise to some effect.

$v_C/T_C > \zeta_{\text{sph}}(T_C)$  region is presented in the right panel of Fig. 9.  $\alpha \lesssim -14.7^\circ$  is needed



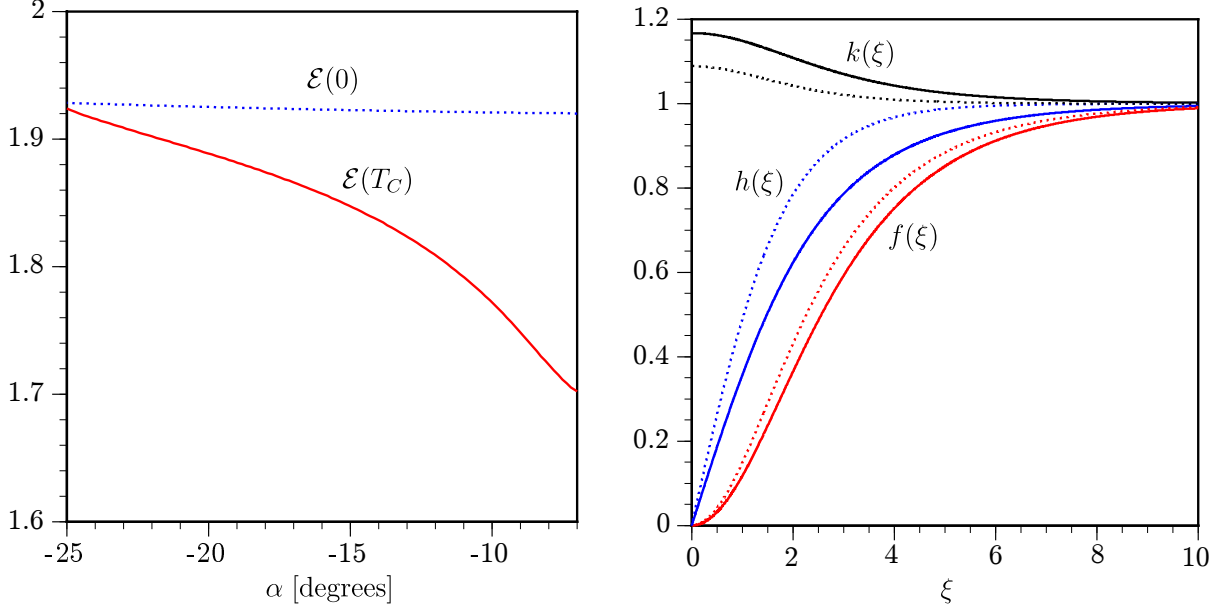


FIG. 8. (Left panel)  $\mathcal{E}(T_C)$  and  $\mathcal{E}(0)$  are shown as a function of  $\alpha$ . (Right panel) The sphaleron profiles are plotted as a function of  $\xi$  at  $T = 0$  GeV and  $T = T_C$ , where we take  $\alpha = -10^\circ$ . The straight (dotted) lines denote  $f(\xi)$ ,  $h(\xi)$  and  $k(\xi)$  at  $T = T_C(0)$  GeV.

to archive the successful sphaleron decoupling. On the other hand,  $\alpha \lesssim -12.9^\circ$  is obtained if  $v_C/T_C > 1$  is used.

### C. Triple Higgs boson coupling

We investigate a correlation between the triple Higgs boson coupling ( $\lambda_{H_1 H_1 H_1}$ ) and the strength of the strong first-order EWPT (for a tree level analysis in the rSM, see [36]). To do so, we evaluate  $\lambda_{H_1 H_1 H_1}$  in the effective potential approach. Although the external momentum dependence is inherently important, we do not pursue this analysis in this paper and defer it to future work.  $\lambda_{H_1 H_1 H_1}^{\text{rSM}}$  at the one-loop order is given by

$$\lambda_{H_1 H_1 H_1}^{\text{rSM}} = \lambda_{H_1 H_1 H_1}^{\text{rSM,tree}} + \lambda_{H_1 H_1 H_1}^{\text{rSM,loop}}, \quad (44)$$

where

$$\lambda_{H_1 H_1 H_1}^{\text{rSM,tree}} = 6 \left[ \lambda_H v c_\alpha^3 + \frac{\mu_{HS}}{2} s_\alpha c_\alpha^2 + \frac{\lambda_{HS}}{2} s_\alpha c_\alpha (v s_\alpha + v_S c_\alpha) + \left( \frac{\mu'_S}{3} + \lambda_S v_S \right) s_\alpha^3 \right], \quad (45)$$

$$\lambda_{H_1 H_1 H_1}^{\text{rSM,loop}} = c_\alpha^3 \left\langle \frac{\partial^3 V_1}{\partial \varphi_H^3} \right\rangle + c_\alpha^2 s_\alpha \left\langle \frac{\partial^3 V_1}{\partial \varphi_H^2 \partial \varphi_S} \right\rangle + c_\alpha s_\alpha^2 \left\langle \frac{\partial^3 V_1}{\partial \varphi_H \partial \varphi_S^2} \right\rangle + s_\alpha^3 \left\langle \frac{\partial^3 V_1}{\partial \varphi_S^3} \right\rangle, \quad (46)$$

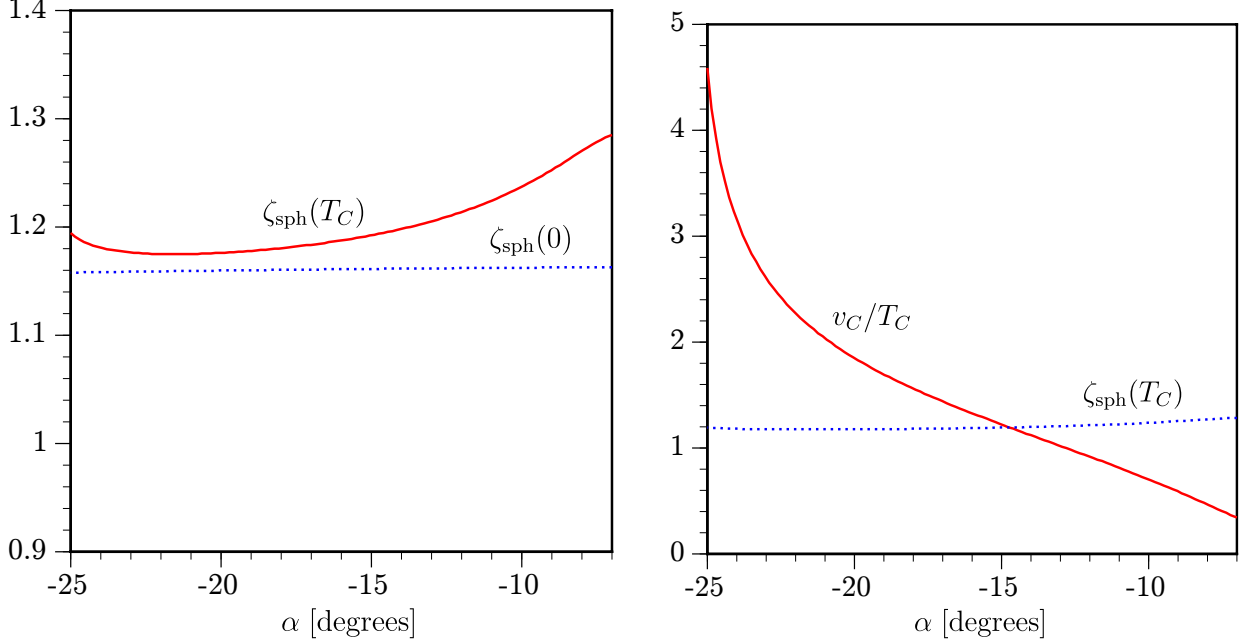


FIG. 9. (Left panel)  $\zeta_{\text{sph}}$  at  $T_C$  and 0 are plotted as a function of  $\alpha$ . (Right panel)  $v_C/T_C$  vs.  $\zeta_{\text{sph}}$  in the same  $\alpha$  range as the left panel.

where  $c_\alpha = \cos \alpha$  and  $s_\alpha = \sin \alpha$ . It should be noted that the vacuum and Higgs boson masses have to be renormalized at the one-loop level in order to evaluate  $\lambda_{H_1 H_1 H_1}^{\text{rSM}}$  properly. In our analysis, Eqs. (38) - (41) are used for it. One can easily work out  $\lambda_{H_1 H_1 H_1}$  in the SM in the effective potential approach (see, e.g., [37]). In this case,  $\lambda_{H_1 H_1 H_1}$  has the simple form

$$\lambda_{H_1 H_1 H_1}^{\text{SM}} = \frac{3m_{H_1}^2}{v} \left[ 1 + \frac{9m_{H_1}^2}{32\pi^2 v^2} + \sum_{i=W,Z,t,b} n_i \frac{m_i^4}{12\pi^2 m_{H_1}^2 v^2} \right] \simeq 175.83 \text{ [GeV]}. \quad (47)$$

Note that the largest one-loop contribution comes from the top quark loop and it grows as  $\mathcal{O}(m_t^4)$ . Such a nondecoupling effect can also appear in the radiative corrections to the triple Higgs boson coupling in the two Higgs doublet model [37] and some class of the supersymmetric models [38].

We define the deviation of the triple Higgs boson coupling from the SM value as

$$\Delta\lambda_{H_1 H_1 H_1} = \frac{\lambda_{H_1 H_1 H_1}^{\text{rSM}} - \lambda_{H_1 H_1 H_1}^{\text{SM}}}{\lambda_{H_1 H_1 H_1}^{\text{SM}}}. \quad (48)$$

In Fig. 10, a relationship between  $\kappa$  and  $\Delta\lambda_{H_1 H_1 H_1}$  are shown in the strong first-order EWPT region. The input parameters are the same as those in Fig. 7. It is found that  $\kappa \lesssim 0.97$  and  $\Delta\lambda_{H_1 H_1 H_1} \gtrsim 17.5 \%$ , where the lower values correspond to the case  $v_C/T_C \simeq 1.20$

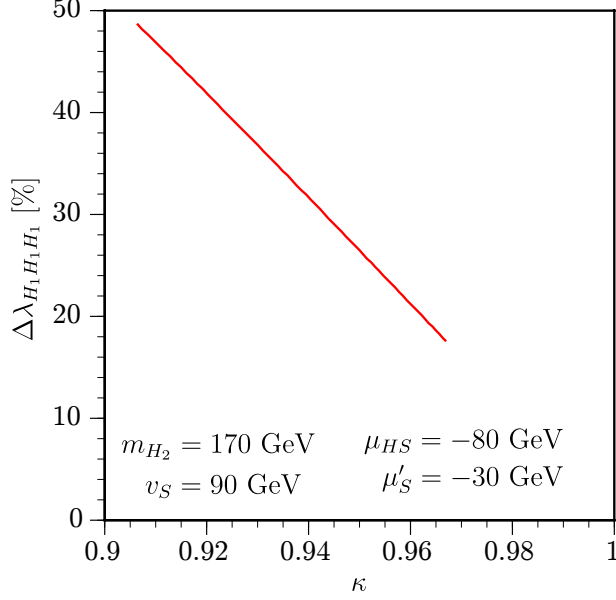


FIG. 10.  $\kappa$  and  $\Delta\lambda_{H_1 H_1 H_1}$  in the strong first-order EWPT region. The right end point of the red line corresponds to  $v_C/T_C \simeq 1.20$  and  $\zeta_{\text{sph}}(T_C) \simeq 1.19$  while  $v_C/T_C \simeq 4.59$  and  $\zeta_{\text{sph}}(T_C) \simeq 1.19$  at the left end point.

and  $\zeta_{\text{sph}}(T_C) \simeq 1.19$ .  $\Delta\lambda_{H_1 H_1 H_1}$  can be as large as 48.7% at  $\kappa \simeq 0.91$ , where  $v_C/T_C \simeq 4.59$  and  $\zeta_{\text{sph}}(T_C) \simeq 1.19$  as shown in the right panel of Fig. 9.

We study  $\Delta\lambda_{H_1 H_1 H_1}$  in larger regions by varying  $m_{H_2}$ . Our finding is presented in Fig. 11.  $\Delta\lambda_{H_1 H_1 H_1}$  is overlaid on the same plane as in Fig. 6 but with  $\kappa$  rather than  $\alpha$  for the vertical axis.  $\Delta\lambda_{H_1 H_1 H_1} = 10, 20, 30, 50$  and 100% contours are plotted with the dotted lines from top to bottom. To stand out how much the sphaleron decoupling condition is improved,  $v_C/T_C = 1$  line is also displayed with a blue color. For some representative points in the successful EWBG region, we find that

- $\Delta\lambda_{H_1 H_1 H_1} \simeq 16\%$  for  $\kappa \simeq 0.97$  and  $160 \text{ GeV} \lesssim m_{H_2} \lesssim 169 \text{ GeV}$ .
- $\Delta\lambda_{H_1 H_1 H_1} \simeq 27\%$  for  $\kappa \simeq 0.95$ , and  $163 \text{ GeV} \lesssim m_{H_2} \lesssim 176 \text{ GeV}$ .
- $\Delta\lambda_{H_1 H_1 H_1} \simeq 50\%$  for  $\kappa \simeq 0.90$ , and  $170 \text{ GeV} \lesssim m_{H_2} \lesssim 206 \text{ GeV}$ .

It should be emphasized that the upper bound of  $m_{H_2}$  in each case is enlarged to 172, 182 and 227 GeV, respectively, if  $v_C/T_C > 1$  is used as the sphaleron decoupling condition. On the other hand, for a fixed  $m_{H_2}$  with  $\kappa < 0.9$ ,  $\Delta\lambda_{H_1 H_1 H_1}$  gets reduced by up to about 8% once we adopt  $v_C/T_C > 1$ .

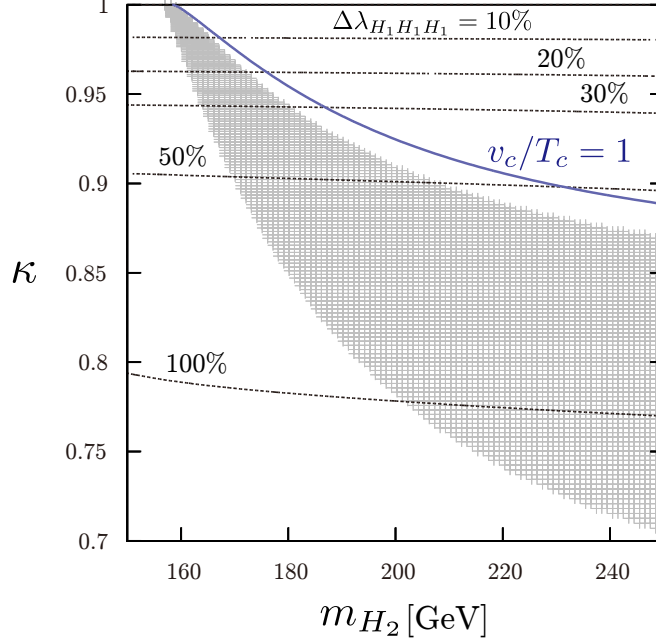


FIG. 11.  $\Delta\lambda_{H_1 H_1 H_1}$  in the  $(m_{H_2}, \kappa)$  plane. The input parameters are the same as in Fig. 6.  $v_C/T_C > \zeta_{\text{sph}}(T_C)$  is satisfied in the shaded region. For a reference,  $v_C/T_C = 1$  contour line is also shown.

Here, we comment on the Landau pole issue. As we have studied in this section, to satisfy the sphaleron decoupling condition the Higgs portal coupling ( $\lambda_{HS}$ ) has to be greater than the certain values, which may hit the Landau pole below the grand unification scale ( $\simeq 2 \times 10^{16}$  GeV). To examine this, we solve the renormalization group equations of  $\lambda_{H,S,HS}$  (for one-loop  $\beta$  functions, see, i.e., [14]). We determine the cutoff ( $\Lambda$ ) of the model by a scale at which  $\lambda_{H,S,HS}(\Lambda) > 4\pi$  occurs. In our explored parameter space,  $\Lambda$  cannot reach the grand unification scale in the successful EWBG region. We obtain  $\Lambda \lesssim 10^4$  GeV in Case (i) and  $\Lambda \lesssim 10^{14}$  GeV in Case (ii).

Finally, our benchmark points are summarized in Table II. S1 and S2 have been already discussed in this section. S3 and S4 are newly exemplified as a reference. In S3, although the strong first-order EWPT is possible, no significant deviations appear in the Higgs coupling constants since  $\alpha = 0$ . Such a specific case was pointed out in [15], and may be probed by the gravitational wave as discussed there. In S4, the Higgs portal parameter is only nonzero  $\mu_{HS}$ . Unlike S1,  $\alpha$  is not necessarily large in order to induce the strong first-order EWPT. However,  $\lambda_S$  is so large that  $\Lambda$  cannot go beyond 10 TeV. The low  $\Lambda$  is the common feature

	S1	S2	S3	S4
H-S mixing parameters	$\lambda_{HS}$	$\lambda_{HS}, \mu_{HS}$	$\lambda_{HS}, \mu_{HS}$	$\mu_{HS}$
PT type	D	B	B	B
$m_{H_2}$ [GeV]	500	170	148	500
$\alpha$ [degrees]	38	-20	0	20
$v_S$ [GeV]	200	90	100	200
$\mu_{HS}$ [GeV]	0.00	-80.00	-80.00	-310.72
$\mu'_S$ [GeV]	0	-30	-30	0
$\lambda_H$	0.82	0.13	0.12	0.34
$\lambda_S$	1.83	0.23	0.06	1.96
$\lambda_{HS}$	-2.35	1.08	0.80	0.00
$\kappa$	0.79	0.94	1.0	0.94
$\Delta\lambda_{H_1 H_1 H_1}$ [%]	-23.7	31.8	0.58	41.1
$\log_{10}(\Lambda/\text{GeV})$	3.90	9.68	13.78	3.90
$v_C/T_C$	$\frac{172.83}{148.87} = 1.16$ $\frac{206.75}{111.76} = 1.85$ $\frac{234.78}{79.31} = 2.96$ $\frac{193.40}{120.53} = 1.60$			
$v_{SC}$ [GeV]	145.72	98.31	100.06	182.26
$v_{SC}^{\text{sym}}$ [GeV]	0.00	222.33	436.99	135.40
$\mathcal{E}(T_C)$	1.92	1.89	1.91	1.84
$\zeta_{\text{sph}}(T_C)$	1.14	1.18	1.18	1.20

TABLE II. The benchmark points for the strong first-order EWPT.  $(\lambda_H, \lambda_S, \lambda_{HS})$  are outputs in S1-S3, and  $(\lambda_H, \lambda_S, \mu_{HS})$  are outputs in S4.  $\mu_S = 0$  is taken through out our analysis. For a detail, see a text. S1 is already disfavored by the LHC data and EW precision tests.

of the one Higgs portal parameter scenarios as mentioned above.

## VI. CONCLUSIONS AND DISCUSSION

We have reanalyzed the feasibility of the strong first-order EWPT in the rSM. The sphaleron decoupling condition is improved by taking account of the one-loop corrections at zero and nonzero temperatures. As explicitly shown in this paper, the sphaleron energy gets lowered at high temperatures, and thus the sphaleron decoupling condition becomes more

severe. For moderate values of the model parameters, the sphaleron decoupling condition is found to be  $v_C/T_C > (1.1 - 1.2)$ , which is  $(10 - 20)\%$  more stringent than the conventional one.

We also investigated the impacts of the improved sphaleron decoupling condition on the deviations of the Higgs coupling constants from the SM values. In a typical case, if the Higgs couplings to the gauge bosons/fermions deviate from the SM values by about 3 (10)%, the deviation of the triple Higgs boson coupling can be as large as about 16 (50)%, which is about 4 (8)% larger than that based on the conventional criterion  $v_C/T_C > 1$ . It is also found that the ranges of  $m_{H_2}$  that is consistent with the successful sphaleron decoupling get limited by certain amounts depending on the magnitude of  $\kappa$ . For  $\kappa \simeq 0.90$ , we observe that the upper bound of  $m_{H_2}$  is reduced by about 20 GeV if the refined sphaleron decoupling condition is used.

Apart from  $\alpha = 0$  case as in S3, the significant deviations from the SM values show up in the Higgs coupling constants if the EWPT is strongly first order. Such deviations can be probed at the high-luminosity LHC [39] and the international linear collider [40].

Finally, we comment on some remaining issues. In order to reduce the theoretical uncertainties in the sphaleron decoupling condition, we should include the sub-leading contributions omitted here. For example, the translational and rotational zero-mode factors around the sphaleron can have some effects, leading to the enhanced  $\zeta_{\text{sph}}$ . In addition,  $T_C$  has to be replaced with  $T_N$  in the sphaleron decoupling condition. Since some regions in the parameter space show the significantly large  $v_C/T_C$ , the corresponding supercooling can be sizable, which delays the onset of the EWPT. If the EWPT mostly proceeds via the bubble nucleation rather than bubble expansion, the EWBG mechanism might not work. If this is the case, we may obtain the upper bound of the size of  $v_C/T_C$ , rendering the feasible regions more limited.

In order to incorporate new  $CP$  violation, the current model has to be extended. As long as new particles do not affect the EWPT significantly, the current analysis would be valid.

## ACKNOWLEDGMENTS

We thank Junji Hisano and Natsumi Nagata for variable comments.

- 
- [1] G. Aad *et al.* [ATLAS Collaboration], Phys. Lett. B **716**, 1 (2012) [arXiv:1207.7214 [hep-ex]].
  - [2] S. Chatrchyan *et al.* [CMS Collaboration], Phys. Lett. B **716**, 30 (2012) [arXiv:1207.7235 [hep-ex]].
  - [3] J. Beringer *et al.* [Particle Data Group Collaboration], Phys. Rev. D **86**, 010001 (2012).
  - [4] A. D. Sakharov, Pisma Zh. Eksp. Teor. Fiz. **5**, 32 (1967) [JETP Lett. **5**, 24 (1967 SOPUA,34,392-393.1991 UFNAA,161,61-64.1991)].
  - [5] K. Kajantie, M. Laine, K. Rummukainen and M. E. Shaposhnikov, Phys. Rev. Lett. **77**, 2887 (1996); K. Rummukainen, M. Tsypin, K. Kajantie, M. Laine and M. E. Shaposhnikov, Nucl. Phys. B **532**, 283 (1998); F. Csikor, Z. Fodor and J. Heitger, Phys. Rev. Lett. **82**, 21 (1999); Y. Aoki, F. Csikor, Z. Fodor and A. Ukawa, Phys. Rev. D **60**, 013001 (1999).
  - [6] N. Cabibbo, Phys. Rev. Lett. **10**, 531 (1963).
  - [7] M. Kobayashi and T. Maskawa, Prog. Theor. Phys. **49**, 652 (1973).
  - [8] M. B. Gavela, P. Hernandez, J. Orloff and O. Pene, Mod. Phys. Lett. A **9** (1994) 795; M. B. Gavela, P. Hernandez, J. Orloff, O. Pene and C. Quimbay, Nucl. Phys. B **430** (1994) 382; P. Huet and E. Sather, Phys. Rev. D **51** (1995) 379; T. Konstandin, T. Prokopec and M. G. Schmidt, Nucl. Phys. B **679** (2004) 246.
  - [9] V. A. Kuzmin, V. A. Rubakov and M. E. Shaposhnikov, Phys. Lett. B **155** (1985) 36. For reviews on electroweak baryogenesis, see A. G. Cohen, D. B. Kaplan and A. E. Nelson, Ann. Rev. Nucl. Part. Sci. **43** (1993) 27; M. Quiros, Helv. Phys. Acta **67** (1994) 451; V. A. Rubakov and M. E. Shaposhnikov, Usp. Fiz. Nauk **166** (1996) 493; K. Funakubo, Prog. Theor. Phys. **96** (1996) 475; M. Trodden, Rev. Mod. Phys. **71** (1999) 1463; W. Bernreuther, Lect. Notes Phys. **591** (2002) 237; J. M. Cline, [arXiv:hep-ph/0609145]; D. E. Morrissey and M. J. Ramsey-Musolf, New J. Phys. **14**, 125003 (2012); T. Konstandin, arXiv:1302.6713 [hep-ph].
  - [10] T. Cohen, D. E. Morrissey and A. Pierce, Phys. Rev. D **86**, 013009 (2012); D. Curtin, P. Jaiswal and P. Meade, JHEP **1208**, 005 (2012); M. Carena, G. Nardini, M. Quiros and C. E. M. Wagner, JHEP **1302**, 001 (2013); K. Krizka, A. Kumar and D. E. Morrissey,

- arXiv:1212.4856 [hep-ph].
- [11] K. Funakubo and E. Senaha, Phys. Rev. D **79**, 115024 (2009) [arXiv:0905.2022 [hep-ph]].
  - [12] Y. Kondo, I. Umemura and K. Yamamoto, Phys. Lett. B **263**, 93 (1991); J. Choi and R. R. Volkas, Phys. Lett. B **317**, 385 (1993) [hep-ph/9308234]; J. R. Espinosa and M. Quiros, Phys. Lett. B **305**, 98 (1993) [hep-ph/9301285]; K. E. C. Benson, Phys. Rev. D **48**, 2456 (1993); J. McDonald, Phys. Lett. B **323**, 339 (1994); G. C. Branco, D. Delepine, D. Emmanuel-Costa and F. R. Gonzalez, Phys. Lett. B **442**, 229 (1998) [hep-ph/9805302]; S. W. Ham, Y. S. Jeong and S. K. Oh, J. Phys. G **31**, 857 (2005) [hep-ph/0411352]; J. M. Cline, G. Laporte, H. Yamashita and S. Kraml, JHEP **0907**, 040 (2009) [arXiv:0905.2559 [hep-ph]]; S. Das, P. J. Fox, A. Kumar and N. Weiner, JHEP **1011**, 108 (2010) [arXiv:0910.1262 [hep-ph]]; D. J. H. Chung and A. J. Long, Phys. Rev. D **84**, 103513 (2011) [arXiv:1108.5193 [astro-ph.CO]]; J. R. Espinosa, B. Gripaios, T. Konstandin and F. Riva, JCAP **1201**, 012 (2012) [arXiv:1110.2876 [hep-ph]]; M. Fairbairn and R. Hogan, JHEP **1309**, 022 (2013) [arXiv:1305.3452 [hep-ph]]; T. Li and Y. -F. Zhou, arXiv:1402.3087 [hep-ph].
  - [13] S. Profumo, M. J. Ramsey-Musolf and G. Shaughnessy, JHEP **0708**, 010 (2007) [arXiv:0705.2425 [hep-ph]].
  - [14] M. Gonderinger, Y. Li, H. Patel and M. J. Ramsey-Musolf, JHEP **1001**, 053 (2010) [arXiv:0910.3167 [hep-ph]].
  - [15] A. Ashoorioon and T. Konstandin, JHEP **0907**, 086 (2009) [arXiv:0904.0353 [hep-ph]].
  - [16] J. R. Espinosa, T. Konstandin and F. Riva, Nucl. Phys. B **854**, 592 (2012) [arXiv:1107.5441 [hep-ph]].
  - [17] J. M. Cline and K. Kainulainen, JCAP **1301**, 012 (2013) [arXiv:1210.4196 [hep-ph]].
  - [18] S. Kanemura, Y. Okada and E. Senaha, Phys. Lett. B **606**, 361 (2005) [hep-ph/0411354].
  - [19] K. Funakubo, S. Tao and F. Toyoda, Prog. Theor. Phys. **114**, 369 (2005) [hep-ph/0501052].
  - [20] S. R. Coleman and E. J. Weinberg, Phys. Rev. D **7**, 1888 (1973).
  - [21] R. Jackiw, Phys. Rev. D **9**, 1686 (1974).
  - [22] L. Dolan and R. Jackiw, Phys. Rev. D **9**, 3320 (1974).
  - [23] M. E. Carrington, Phys. Rev. D **45**, 2933 (1992).
  - [24] P. B. Arnold and L. D. McLerran, Phys. Rev. D **36**, 581 (1987).
  - [25] N. S. Manton, Phys. Rev. D **28**, 2019 (1983).



- [26] F. R. Klinkhamer and N. S. Manton, Phys. Rev. D **30**, 2212 (1984).
- [27] K. Funakubo, A. Kakuto, S. Tao and F. Toyoda, Prog. Theor. Phys. **114**, 1069 (2006) [arXiv:hep-ph/0506156].
- [28] B. M. Kastening and X. Zhang, Phys. Rev. D **45**, 3884 (1992); J. Choi, Phys. Lett. B **345**, 253 (1995) [hep-ph/9409360]; A. Ahriche, Phys. Rev. D **75**, 083522 (2007) [hep-ph/0701192].
- [29] B. Kleihaus, J. Kunz and Y. Brihaye, Phys. Lett. B **273**, 100 (1991); F. R. Klinkhamer and R. Laterveer, Z. Phys. C **53**, 247 (1992).
- [30] Y. .B. Zeldovich, I. Y. .Kobzarev and L. B. Okun, Zh. Eksp. Teor. Fiz. **67**, 3 (1974) [Sov. Phys. JETP **40**, 1 (1974)].
- [31] M. E. Peskin and T. Takeuchi, Phys. Rev. Lett. **65**, 964 (1990).
- [32] I. Maksymyk, C. P. Burgess and D. London, Phys. Rev. D **50**, 529 (1994) [hep-ph/9306267].
- [33] S. Baek, P. Ko, W. -I. Park and E. Senaha, JHEP **1211**, 116 (2012) [arXiv:1209.4163 [hep-ph]].
- [34] ATLAS collaboration, Updated coupling measurements of the Higgs boson with the ATLAS detector using up to  $25 \text{ fb}^{-1}$  of proton-proton collision data, ATLAS-CONF-2014-009.
- [35] CMS collaboration, Combination of standard model Higgs boson searched and measurements of the properties of the new boson with a mass near 125 GeV, CMS-PAS-HIG-13-004.
- [36] A. Noble and M. Perelstein, Phys. Rev. D **78**, 063518 (2008) [arXiv:0711.3018 [hep-ph]].
- [37] S. Kanemura, S. Kiyoura, Y. Okada, E. Senaha and C. P. Yuan, Phys. Lett. B **558**, 157 (2003); S. Kanemura, Y. Okada, E. Senaha and C. -P. Yuan, Phys. Rev. D **70**, 115002 (2004) [hep-ph/0408364].
- [38] S. Kanemura, E. Senaha, T. Shindou and T. Yamada, JHEP **1305**, 066 (2013) [arXiv:1211.5883 [hep-ph]].
- [39] [ ATLAS Collaboration], “Physics at a High-Luminosity LHC with ATLAS,” arXiv:1307.7292 [hep-ex].
- [40] H. Baer, T. Barklow, K. Fujii, Y. Gao, A. Hoang, S. Kanemura, J. List and H. E. Logan *et al.*, arXiv:1306.6352 [hep-ph].